Journal of
Ceramic Science
and Technology

*J. Ceram. Sci. Technol.*, **08** [2] 213-222 (2017)
DOI: 10.4416/JCST2016-00086
available online at: http://www.ceramic-science.com
© 2017 Göller Verlag

# Manufacture and Tribological Behavior of C/C-SiC Brake Composites Modified with Fe-Si Alloy

**Y-H. Lu[1], Z. Li[1, 2], W. Zhou[1], P. Xiao[*1]**

[1]State Key Laboratory of Powder Metallurgy, Central South University, Changsha 410083, PR China
[2]College of Metallurgical Engineering, Hunan University of Technology, Zhuzhou 412008, P R China

received October 20, 2016; received in revised form December 27, 2016; accepted February 17, 2017

**Abstract**

**To obtain a stable coefficient of friction (COF) for C/C-SiC composites at high brake speed, simultaneous infiltration of molten Si and Fe alloy into needled C/C materials was developed for fabricating C/C-SiC composites. Consequently, the effect of Fe-Si alloy on the mechanical properties and tribological behavior of C/C-SiC composites was investigated in this work. The results showed that the C/C-SiC composites were composed of C, SiC, FeSi and $FeSi_2$, respectively. Furthermore, the SiC and Fe-Si alloy were mainly distributed in short woven web cloth and among fiber bundles. C/C-SiC composites modified with Fe-Si alloy exhibited lower compressive and flexural strength. Additionally, the brake curve was smoother, while the wear rate was higher. This indicates that introducing Fe-Si alloy into the matrix can impair the mechanical properties, and increase the wear rate, but also improve the friction curve. The typical brake curves were in the shape of a horse saddle.**

*Keywords: C/C-SiC, friction, wear*

## I. Introduction

Carbon-fiber-reinforced carbon and silicon carbide binary matrix (C/C-SiC) composites are a new type of high-performance brake materials developed after C/C composites [1–3]. Compared to C/C composites, C/C-SiC composites exhibit lower sensitivity to their surroundings and temperature in combination with high thermal shock resistance and longer service life [2,4]. Today, therefore, C/C-SiC composites are one of the best candidates for advanced friction materials in the future [5–7].

C/C-SiC composites were first applied for brake systems in automobiles in the 1990s, and they have already been successfully applied in high-end sport cars like Porsche 911 Turbo, Audi A8, Ferrari Enzo, etc. [3,4,8]. Additionally, Xiao *et al.* [9] have also developed C/C-SiC discs and pads for the brake systems in heavy-duty equipment, e.g. tank and armored vehicles, since 2005. Moreover, the C/C-SiC composites, as the key component in aircraft brake systems, were first installed on some airplanes for trial flight in 2008 [10]. In contrast, no commercial applications in truck or aircraft have been reported to date.

Based on previous investigations, it was found that C/C-SiC composites show an unstable COF at high speed owing to the inhomogeneous composition of the friction pads. Therefore, extensive studies have focused on the composition of C/C-SiC friction pads. Cai *et al.* [11] used a disk-on-disk-type laboratory-scale dynamometer (MM-1000) to test the friction properties of C/C-SiC mated to itself. It was found that the fade of the COF in seawater conditions was significantly reduced when $B_4C$ filler was introduced into the C/C-SiC composites. Zhang *et al.* [12] also used a MM-1000 testing machine to study the tribological properties of C/C-SiC mated to itself. It was perceived that the friction coefficient and friction stability coefficients were both insensitive to the change of brake speed when the C/C-SiC composites were modified with graphite. Furthermore, Fan *et al.* [13] introduced $Ti_3SiC_2$ into C/C-SiC composites, and the tribological properties of C/C-SiC mated to itself were tested in a MM-1000 testing machine. The results showed that the friction stability coefficient was improved. In addition, Li *et al.* [14] introduced nanofiber into C/C-SiC composites, and found that the composites mated to 30CrSiMoVA alloy braked steadily on the MM-1000 testing machine. Li *et al.* [15] also introduced Cu alloy into C/C-SiC composites, and found that a stable COF and low wear rate for C/C-SiC mated to 30CrSiMoVA alloy under low brake speed were obtained. It is well known that Fe, as an essential element, has been widely used in powder metallurgy brake materials because of its excellent tribological properties. Thus, Fan *et al.* [16] applied FeSi75 to modify C/C-SiC composites, and investigated the tribological properties of the composites mated with themselves. Fe and Si powders are more easily accessible than FeSi75, therefore, it would make sense to use Fe and Si powders to modify C/C-SiC composites.

The aim of current work is to obtain a stable coefficient of friction (COF) for C/C-SiC composites at high brake speed. Thus, in this work, the chemical vapor infiltration (CVI) method in combination with liquid infiltration was

* Corresponding author: xiaopengcsu@csu.edu.cn

employed, and the C/C-SiC composites were prepared by means of simultaneous infiltration of molten Si and Fe into needled C/C preforms. The microstructure and mechanical properties were characterized. Moreover, the tribological properties of the C/C-SiC as the stator mated with 30CrSiMoVA steel as the rotator at high speed were investigated .

## II. Material and Methods

### *(1) Preparation of fabrication*

Polyacrylonitrile (PAN)-based carbon fibers (Toray T700, filament of 12 K) were used as reinforcement in the preforms. The diameters and purity of the silicon powder used in this study were 30 – 50 μm and 99.0 %, respectively, according to information supplied by the manufacturer, Beijing Dadi Zelin Silicon Industry Co., Ltd., China. The reduced iron powder (purity 99 %, particle size 40 – 47 μm) was fabricated by Central South University, Changsha, China.

Processing of the investigated C/C-SiC composites modified with Fe-Si alloy consisted of the following three steps. First, the preform was prepared by means of the three-dimensional needling technique, which started with repeatedly overlapping the layers of 0°non-woven fiber cloth, short-cut fiber web, and 90°non-woven fiber cloth by means of needle-punching. The density of the preforms was about 0.55 g $cm^{-3}$.

The second step involved densifying the preforms to get a porous C/C by means of chemical vapor infiltration (CVI). The CVI process was performed at 1000 °C for 100 – 120 h in an argon atmosphere with the absolute pressure of 0.1 MPa. $C_3H_6$ was used as a precursor and $H_2$ as a carrier and diluting gas ($C_3H_6/H_2$=10 ml $min^{-1}$: 20 ml $min^{-1}$). The density of the porous C/C materials was about 1.2 ± 0.05 g $cm^{-3}$.

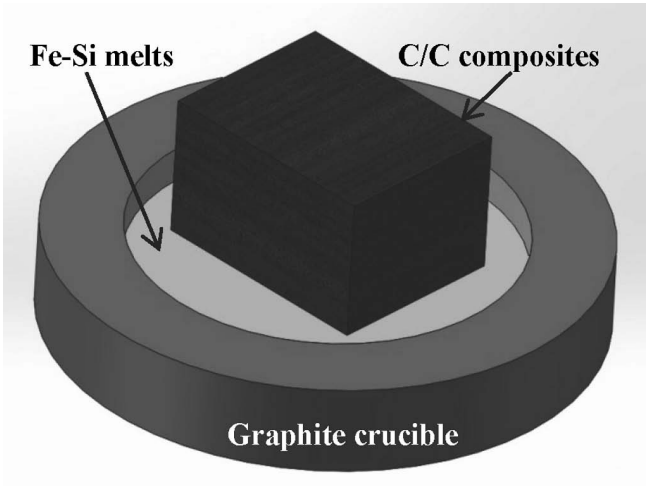


**Fig. 1:** Schematic diagram showing the simultaneous infiltration of molten Fe and Si experiment.

The third step was subsequent infiltration of the resulting porous C/C materials with molten Si and Fe, and a schematic showing this process is shown in Fig. 1. Si and Fe powders were taken with a mass ratio of 60:40 for the infiltration. The infiltration process was conducted at the range of 1700 ± 100 °C with 0.5 – 2 h dwell time under vacuum conditions (absolute pressure < 1 Pa). Thereby, the liquid Si and Fe infiltrated the pores of the C/C materials, and reacted with a small amount of the carbon matrix to form a ceramic matrix.

### *(2) Analysis methods*

The bulk density and open porosity of the samples were measured with Archimedes' method at room temperature (RT). The phases were analyzed by means of X-ray diffraction (XRD, Rigaku D/max 2550 PC) using nickel-filtered CuKα radiation. Thermal diffusivity was tested on a laser flash thermal analyzer (JR-3, China) with the sample size of Ø 10×(3~5) mm. Additionally, a scanning electron microscope (SEM, JEOL JSM-6360LV, Japan) equipped with Energy-Dispersive X-Ray Spectrometer (EDS, Noran Finder 100, America), a polarized light micrograph (PLM, MeF3A) and a three-dimensional rotational digital video microscope (HIROX KH-7700, Japan) were used for structural characterization.

### *(3) Testing of mechanical properties*

The three-point flexural strength test with a support span of 40 mm and a cross-head speed of 0.5 mm/min was conducted on the universal mechanical machine (CSS-44100, Changchun Research Institute for Mechanical Science Co., China) to investigate the flexural property of the as-processed composites. The load direction was perpendicular to the layers of the carbon felt. The sample size was 55 mm × 10 mm × 4 mm. Moreover, the compressive strength of the composites was also determined on the above-mentioned machine with a cross-head speed of 0.5 mm/min by using the sample with the geometry of 10 mm × 10 mm × 10 mm. Note that at least five samples were tested in order to obtain the reliable-mean value for the strength.

### *(4) Test of tribological properties*

The tribological properties were tested on a MM-1000 disc-on-disc type laboratory-scale dynamometer (Xi'an Shuntong Technical Research Institute, China). More details can be found in Ref. [11]. In this work, the C/C-SiC composites modified with Fe-Si alloy acted as the stator, metal-based 30CrSiMoVA alloy as the rotor, and the contacting friction area between the stator and rotor should reach up to about 80 % during running-in before the test. The size of specimens was Ø 75 – 53×15 mm. The given brake speed, brake pressure and inertia were 7500 r $min^{-1}$, 1.0 MPa and 0.1 kg $m^2$ respectively. The COF is calculated automatically by computer. Using Equation (1), the linear wear rate was calculated with the thickness difference of the disk before and after braking tests divided by the braking times. The above test was repeated 20 times and the mean value of the measurements was expressed in the results.

$$\Delta l = \frac{L_1 - L_2}{n} \quad (1)$$

where $L_1$, $L_2$ represents the thickness of the disk before and after the test, respectively, and $n$ is the braking times.

## III. Results and Discussion

### *(1) Phase analysis*

Table 1 presents the general properties for the as-processed composites. It can be seen that the density and open porosity of the C/C-SiC composites modified with Fe-Si alloy are 2.28 g/cm$^3$ and 6.6 %, respectively. This indicates that the Fe-Si alloy has infiltrated well into the porous C/C. Furthermore, thermal diffusivity of the composites at room temperature is 0.26 cm$^2$s$^{-1}$, which is considerably higher than that of the C/C-SiC composites (0.13 cm$^2$ s$^{-1}$). This indicates that thermal properties are improved after infiltration of Fe-Si alloy.

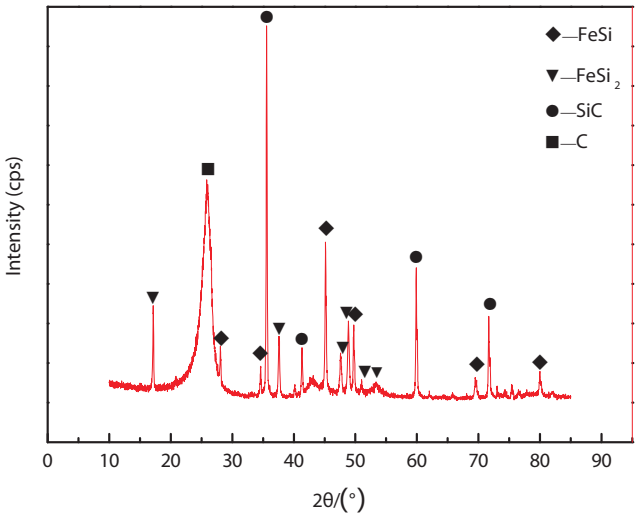


**Fig. 2:** XRD pattern of C/C-SiC composites modified with Fe-Si alloy.

Fig. 2 shows the XRD patterns for the C/C-SiC composites. As shown in Fig. 2, the phases of Fe-Si alloy could be clearly observed in the composites. Moreover, it was found that the composites were composed of approximately 38.6 wt% C, 36.4 wt% SiC, 6.3 wt% FeSi and 18.7 wt% $FeSi_2$, while no residual Si or Fe was detected. Face-centered cubic is the main phase of the SiC, and the carbon phase includes carbon fiber and pyrolytic carbon (PyC). According to the Fe-Si phase diagram [17], only $FeSi_2$ can exist when the mass ratio of Si/Fe is 60/40, the production of FeSi was due to the mass ratio of Si/Fe that goes into every pore and may deviate from 60/40.

### *(2) Microstructure characterization*

Fig. 3 shows the microstructure and element distribution of the C/C-SiC composites modified with Fe-Si alloy. As shown in Fig. 3(a), the composites were composed of the layers of 0° non-woven fiber cloth, short-cut fiber web, 90° non-woven fiber cloth, which were repeatedly overlapped and restricted by needle fibers. There are two types of pores in the porous C/C composites: pores in bundles and pores adjacent to bundles. During the infiltration process, the internal pores in the bundles are too small to be infiltrated. Conversely, the pores adjacent to bundles are big enough to facilitate flowing of Fe-Si melt. Thus, pores within both the interbundle and interply regions could act as a communicating channel for the Fe-Si melt. Consequently, SiC, FeSi and $FeSi_2$ are mainly distributed in the short fiber web layers and the interbundle regions.

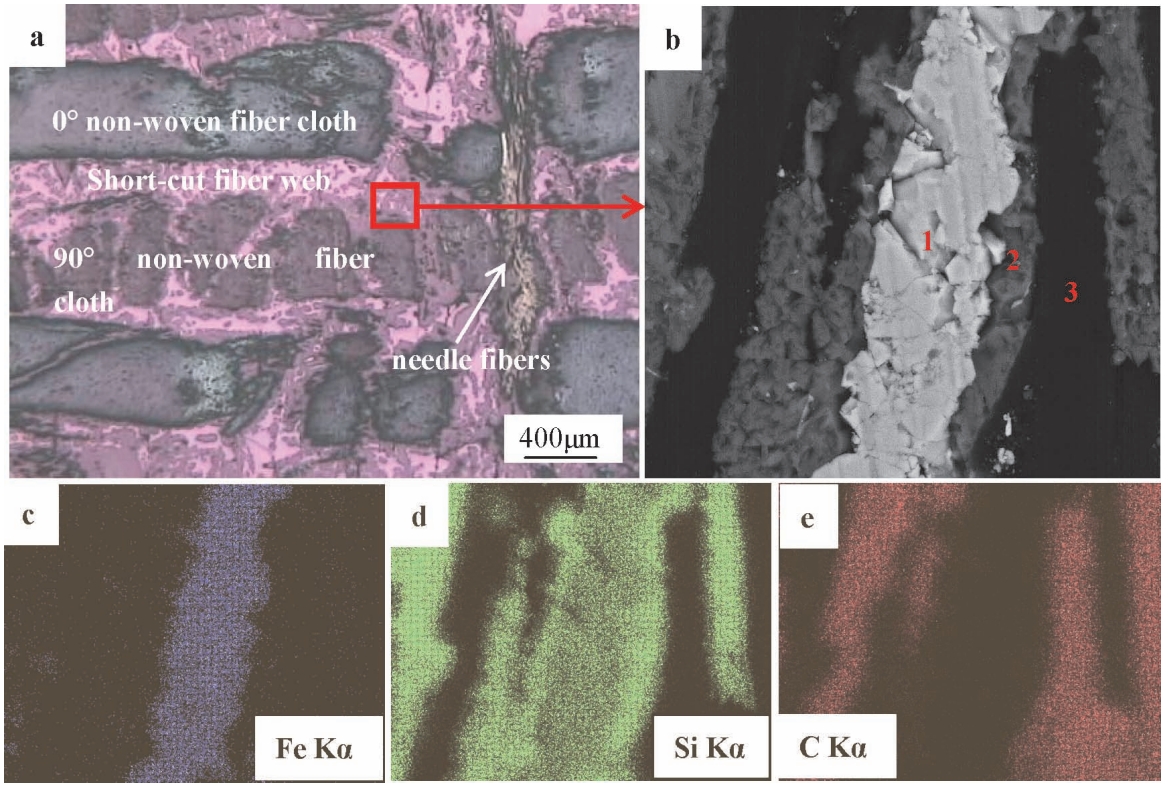


**Fig. 3:** Microstructure and element distribution of C/C-SiC composites modified with Fe-Si alloy: (a) Polarized light optical microstructure; (b) SEM morphology; (c) Fe distribution; (d) Si distribution; (e) C distribution.

**Table 1:** Physical properties of the C/C-SiC composites modified with Fe-Si alloy.

| C/C-SiC | Si : Fe (wt) | Density (g/cm$^3$) | | Open porosity (%) | Thermal diffusivity (cm$^2$/s) |
|---|---|---|---|---|---|
| | | Before infiltration | After infiltration | | |
| Modified with Fe-Si alloy | 60:40 | 1.32 (0.05) | 2.28 (0.1) | 6.6 (1.2) | 0.26 (0.02) |

Standard deviations are given in parentheses.

**Table 2:** Mechanical properties of the C/C-SiC composites modified with Fe-Si alloy.

| C/C-SiC composites | Flexural strength (MPa) | Flexural modulus (GPa) | Strain (%) | Compressive strength (MPa) |
|---|---|---|---|---|
| Modified with Fe-Si alloy | 189.7 (20) | 21.6 (2.2) | 1.32 (0.2) | 296.9 (15) |

Standard deviations are given in parentheses.

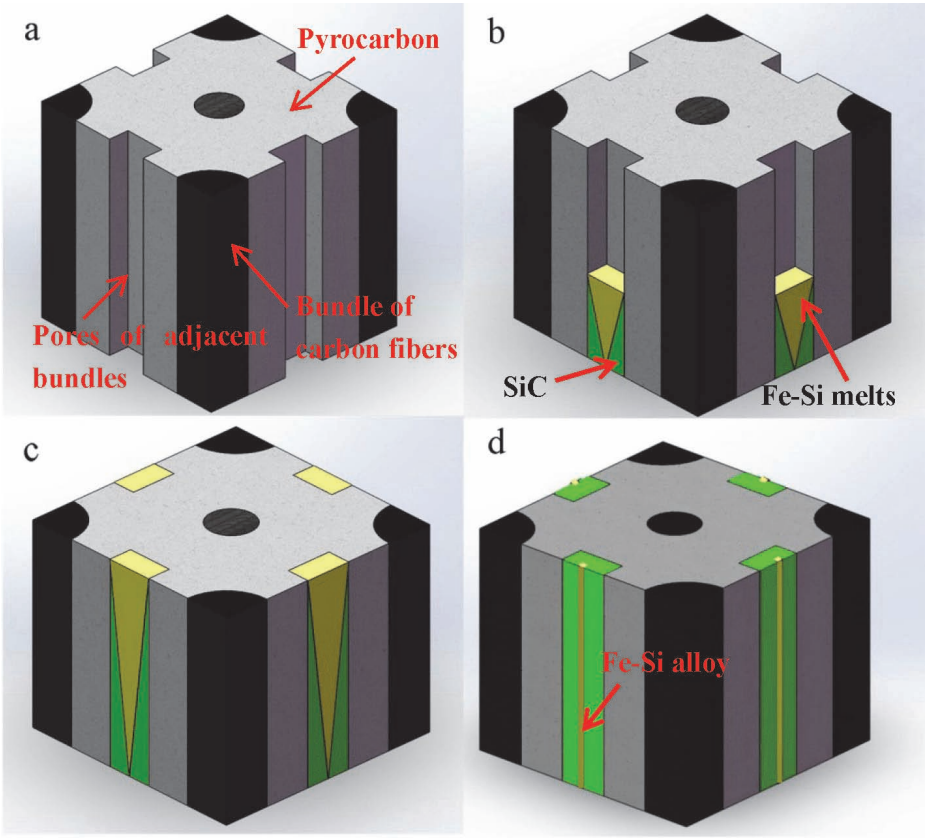


**Fig. 4:** Schematic showing infiltration mechanisms of Fe-Si melt in porous C/C composites: (a) structure of infiltration; (b) initial stage of infiltration; (c) middle stage of infiltration; (d) final stage of infiltration.

In order to fully understand the distribution of different phases, area scanning EDS element analysis was used to investigate the element distribution among the carbon fiber bundles. Three different kinds of phases can be identified in Fig. 3(b). Based on the element distribution (Fig. 3(c-e)), it can be deduced that the light white phase is Fe-Si alloy (marked as 1), the gray phase distributed next to Fe-Si alloy is SiC (marked as 2), and the black phase is identified as carbon (marked as 3). Note that the Fe-Si alloy is distributed between the SiC and SiC. The particular morphology was attributed to the good wetting ability between Fe-Si alloy and SiC [18,19].

Based on the microstructure, a schematic of the infiltration mechanism of the Fe-Si melt was drawn up and is shown in Fig. 4. Infiltration processing can be divided into three stages. Initially, the Fe-Si melt goes into the capillary tube of C/C, and Si reacts with C to form SiC, as shown in Fig. 4(b). The formation of SiC helps the melt go through the tube. In the second stage, shown in Fig. 4(c), the Fe-Si melt climbs higher to an extreme height with the increase in the height of the SiC layer. Finally, as shown in Fig. 4(d),

the melt does not flow, and C atoms diffuse into the melt through the formed SiC layer to react with Si, forming new SiC. The newly formed SiC precipitates on the formed SiC. When sample cooled down, residue Fe-Si alloy solidified in the form of FeSi and $FeSi_2$. Infiltration reactions are described by the following chemical equations:

$$Si(l) + C(s) \rightarrow SiC(s) \quad (2)$$

$$Si(l) + Fe(l) \rightarrow FeSi_2(l) \quad (3)$$

$$Si(l) + Fe(l) \rightarrow FeSi(l) \quad (4)$$

It should be noted that no $Fe_3C$ is formed. According to the dissolution-precipitation forming mechanism of SiC in Ref. [20,21], C atoms could diffuse into the Fe-Si melt through the formed SiC layer. When Fe atoms encounter C atoms, it is possible for $Fe_3C$ to form, driven by thermodynamics. The fact that $Fe_3C$ did not form can be explained by the absence of suitable kinetic conditions. As a result, C atoms are prone to react with Si to form SiC, and Fe atoms are also inclined to react with Si to form FeSi and $FeSi_2$.

### *(3) Mechanical properties*

The mechanical properties of the C/C-SiC composites modified with Fe-Si alloy are shown in Table 2. The mean flexural strength of the C/C-SiC composites modified with Fe-Si alloy is 189.7 ± 20 MPa, which is somewhat lower than that of the C/C-SiC composites (214.6 ± 20 MPa). In addition, the compressive strength of the former is 296.9 ±15 MPa, which is also lower than that of the C/C-SiC composites (346.6 ± 15 MPa). The results indicate that the introduction of Fe-Si alloy could impair the mechanical properties of C/C-SiC composites. Moreover, the flexural modulus and fracture strain of the modified C/C-SiC composites are about 21.6 GPa and 1.32 %, respectively.

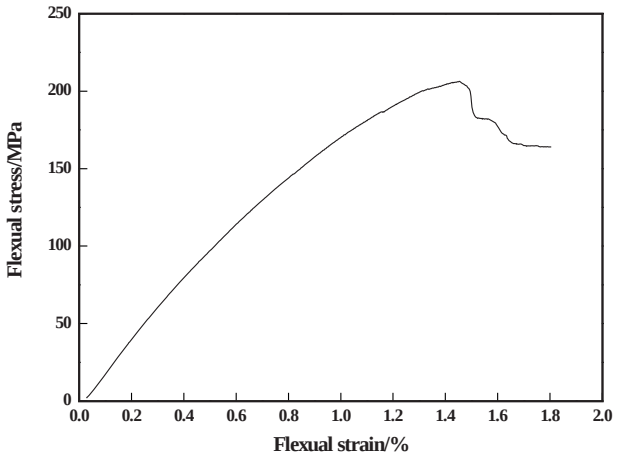


**Fig. 5:** Flexural stress-strain curve of C/C-SiC composites modified with Fe-Si alloy.

Fig. 5 shows the typical fracture behavior of C/C-SiC composites modified with Fe-Si alloy subjected to flexural loading. Initially, the flexural stress-strain curve displays linear behavior. With the accumulation of damage, the curve displays nonlinear behavior until the maximum stress is reached. The fracture model exhibits a pseudo-plastic characteristic. In general, such a fracture model guarantees that the composites do not suffer catastrophic failure.

It is well known that during loading, the matrix bears the load first, and the load is then transferred to carbon fiber through the interfaces. Three kinds of interfaces exist in C/C-SiC composites modified with Fe-Si alloy. The first one is the carbon fiber/PyC interface, the second one is PyC/SiC, and the third one is SiC/Fe-Si alloy. Generally, the cracks propagated in the following manner. Firstly, the matrix including Fe-Si alloy, SiC and PyC, bore the load together. Owing to the weak SiC/Fe-Si alloy interface, a crack (marked as Crack 1, in Fig. 6(a)) appeared there. With the help of EDS, Fe-Si alloy was confirmed, as shown in Fig. 6(b). Concentrated stress was then released, strain was increased, and load transfer was not influenced. Afterwards, with the increase of load, cracks appeared at the fiber/PyC interface (marked as Crack 2 in Fig. 6(c)) and PyC/SiC interface (marked as Crack 3). Consequently, concentrated stress was released again, and strain was also increased. Load could still be transferred to the carbon fiber effectively. During the process, cracks may also be formed in the matrix, such as the crack in PyC (marked as Crack 4). When load reached the maximum, saturated cracks were produced. Afterwards, owing to so many cracks both at the interfaces and in the matrix, load could not be transferred to the carbon fiber effectively, and small stress could result in strain. At this stage, a large number of fibers were pulled out and holes were left, as shown in Fig. 6(d). The fibers acted to prevent brittle catastrophic failure by providing a number of energy dissipation mechanisms. Clean carbon surface and retained holes indicated a moderate interface between the carbon fiber and PyC, which was beneficial to exert a toughening effect of the carbon fibers. Moreover, crack deflection at the three interfaces and carbon fiber pullout contribute to strengthening and toughening the C/C-SiC composites modified with Fe-Si alloy.

For the C/C-SiC composites modified with Fe-Si alloy, low flexural strength was mainly attributable to the Fe-Si alloy and Fe-Si alloy/SiC interfaces. Compared to SiC, the hardness of Fe-Si alloy is lower. The Vickers microhardness of the Fe-Si alloy was 850, while that of the SiC was 2410 [18]. Low hardness indicated that strength of the Fe-Si alloy was lower than that of SiC. Thus, the Fe-Si alloy cannot bear the same load as the SiC. Moreover, cracks easily occurred at the Fe-Si/SiC interface (as shown in Fig. 6(a)). The cracks easily crossed the interface, which went against strength improvement. As a result, the load could not be delivered efficiently to the carbon fiber by the Fe-Si alloy matrix. In addition, the Fe-Si corroded the carbon fiber and weakened it. As shown in Fig. 7, the Fe-Si alloy located around carbon fiber indicates the existence of carbon fiber corrosion. Taking into account that Si could also corrode carbon fiber in C/C-SiC composites, the low strength of the Fe-Si alloy itself and the weak Fe-Si/SiC interface were the main reasons that led to the lower strength of the C/C-SiC composites modified with Fe-Si alloy.

### *(4) Tribological characteristics*

#### (a) *Friction and wear properties*

The tribological properties of different C/C-SiC brake composites mated with 30CrSiMoVA material are listed in Table 3. Compared with our previous research on

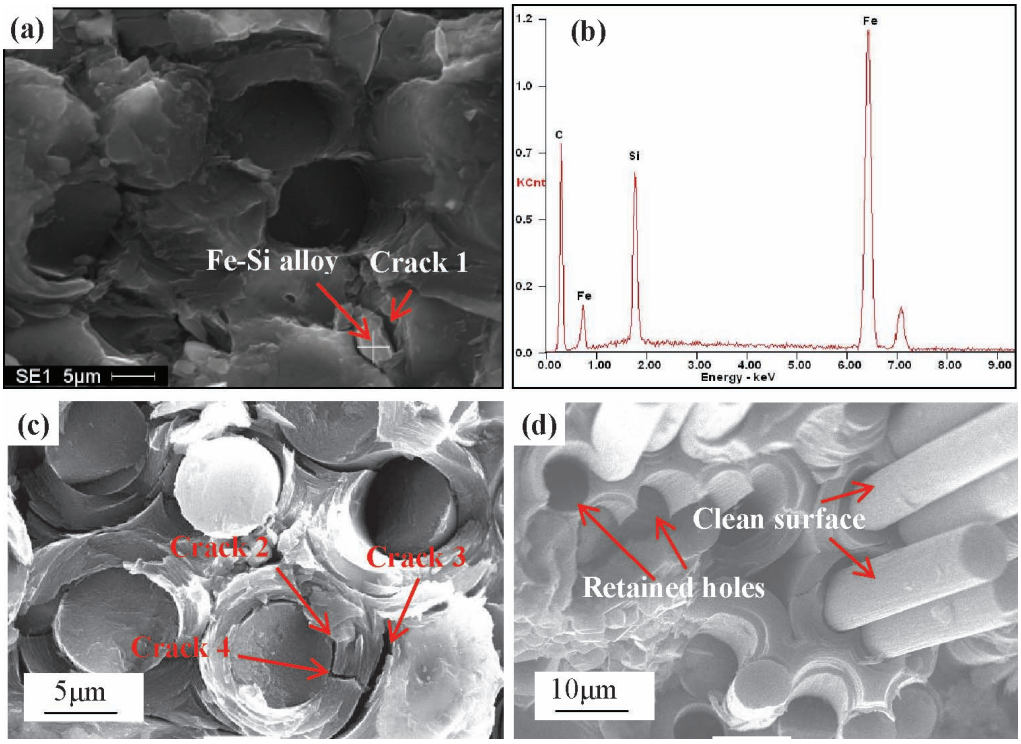


**Fig. 6:** Microscopic fracture profiles of C/C-SiC composites modified by Fe-Si alloy: (a) crack at the Fe-Si/SiC interface; (b) EDS spectrum of Fe-Si alloy in (a); (c) cracks in pyrocarbon, at the interfaces of Cf/carbon and SiC/carbon; (d) fiber pullout.

**Table 3:** Tribological performances of different C/C-SiC composites mated with 30CrSiMoVA counter materials.

| C/C-SiC composites | COF | Temperature of friction subsurface (°C) | Linear wear rate (μm/cycle) | Counterpart wear rate (μm/cycle) |
|---|---|---|---|---|
| Unmodified [6] | 0.25 | 444 | 2.9 | 3.4 |
| Modified with Fe-Si alloy | 0.25 (0.02) | 344 (21) | 3.4 | 3.2 |

Standard deviations are given in parentheses.

unmodified C/C-SiC composites, it indicates that the as-processed composites in this work showed the same friction coefficient, 0.25. The linear wear rate of the C/C-SiC modified with Fe-Si alloy, 3.4 μm cycle$^{-1}$, is higher than that of the C/C-SiC without any modification, 2.9 μm cycle$^{-1}$. Nevertheless, the wear rate of the 30CrSiMoVA counterpart is almost the same.

Typical brake curves of 30CrSiMoVA disk mated with different C/C-SiC composites are shown in Fig. 8. It should be noted that the brake curve of C/C-SiC composites modified with Fe-Si alloy is in the shape of a horse saddle, which presents the typical shape of C/C-SiC composite. At first, pre-up appeared when braking started. Subsequently, the COF decreased with braking time. Finally, approaching the end of brake, tail-up appeared. The same trend of the brake curve was attributed to the same carbon fiber, PyC and SiC matrix. The results indicate that the Fe-Si alloy has not changed the friction mechanism.

Although the average COF of the C/C-SiC composites modified with Fe-Si alloy was the same as that of the C/C-SiC composites, the brake curve was smoother. Moreover, no sharp tail-up appeared. It indicated that the introduction of Fe-Si alloy into the C/C-SiC composites was beneficial to fill in the trough of the COF curve and lower the tail-up crest. The stable COF was ascribed to the low hardness of the Fe-Si alloy, compared to that of the SiC.

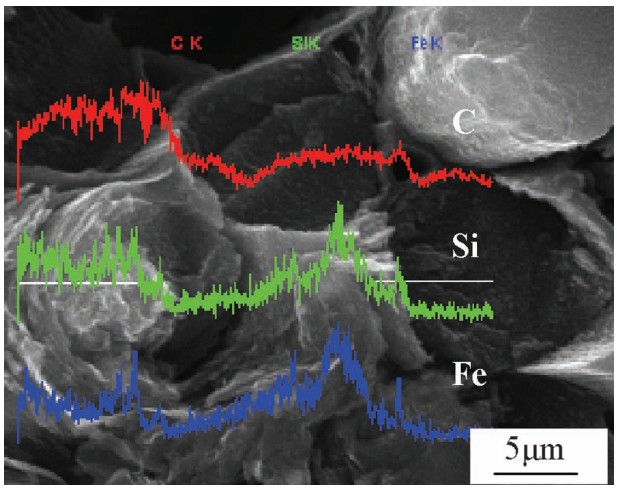


**Fig. 7:** Energy-dispersive analysis of carbon fiber corroded by Fe-Si alloy.

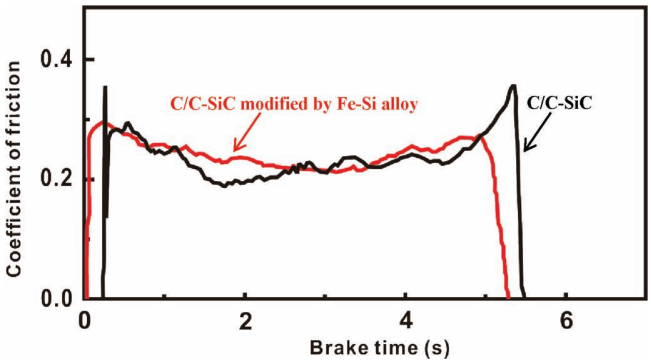


**Fig. 8:** Typical brake curves of different C/C-SiC composites mated with 30CrSiMoVA.

Fluctuation of the braking curve was related to the temperature of the friction surface. When the temperature was high, the braking curve fluctuated too much. In contrast, when the temperature was low, the braking curve was smooth. Tribological performances of different C/C-SiC composites mated with 30CrSiMoVA are listed in Table 3. The sub-surface temperature of the C/C-SiC composites modified with Fe-Si alloy in this work was 344 °C, with 100 °C decrease, compared to that of the unmodified C/C-SiC composites. The Fe-Si alloy had two beneficial effects here. Firstly, the Fe-Si alloy improved the thermal conductivity of the C/C-SiC composite (as shown in Table 1), The produced heat was conducted far away from the friction surface more efficiently, and the friction surface temperature decreased. Secondly, Fe-Si alloy produced more debris, as a result of which more friction heat was taken away. Actually, increasing the wear rate to dissipate friction heat is a popular method used for powder metallurgy brake pads, and the method has been proven to apply to C/C-SiC composite. The wear rate of the as-processed C/C-SiC composites is sufficient for braking material as a car component.

### (b) *Friction surface morphologies*

Generally, the tribological behavior could be characterized by the friction surface [15]. The micrographs of the friction surface for the C/C-SiC composites modified with Fe-Si alloy after the brake test are shown in Fig. 9. Three kinds of wear characteristics: grooves, blue spot and cracks are shown in Fig. 9 (a). In general, grooves are a typical feature caused by abrasive wear. It is known that there is a large number of micro peaks and valleys on the surface of the C/C-SiC composites modified with Fe-Si alloy and metallic counterpart. The micro peaks are generally referred to as asperities. During the brake, the micro peaks and valleys intermeshed with each other, leading to shearing, breaking, and the asperities were embedded into the dual surfaces and plowed into the friction surfaces. Consequently, grooves were left. Moreover, the broken micro asperities, suffering from shearing, will, as a "third body", continue to plow into both friction surfaces [15].

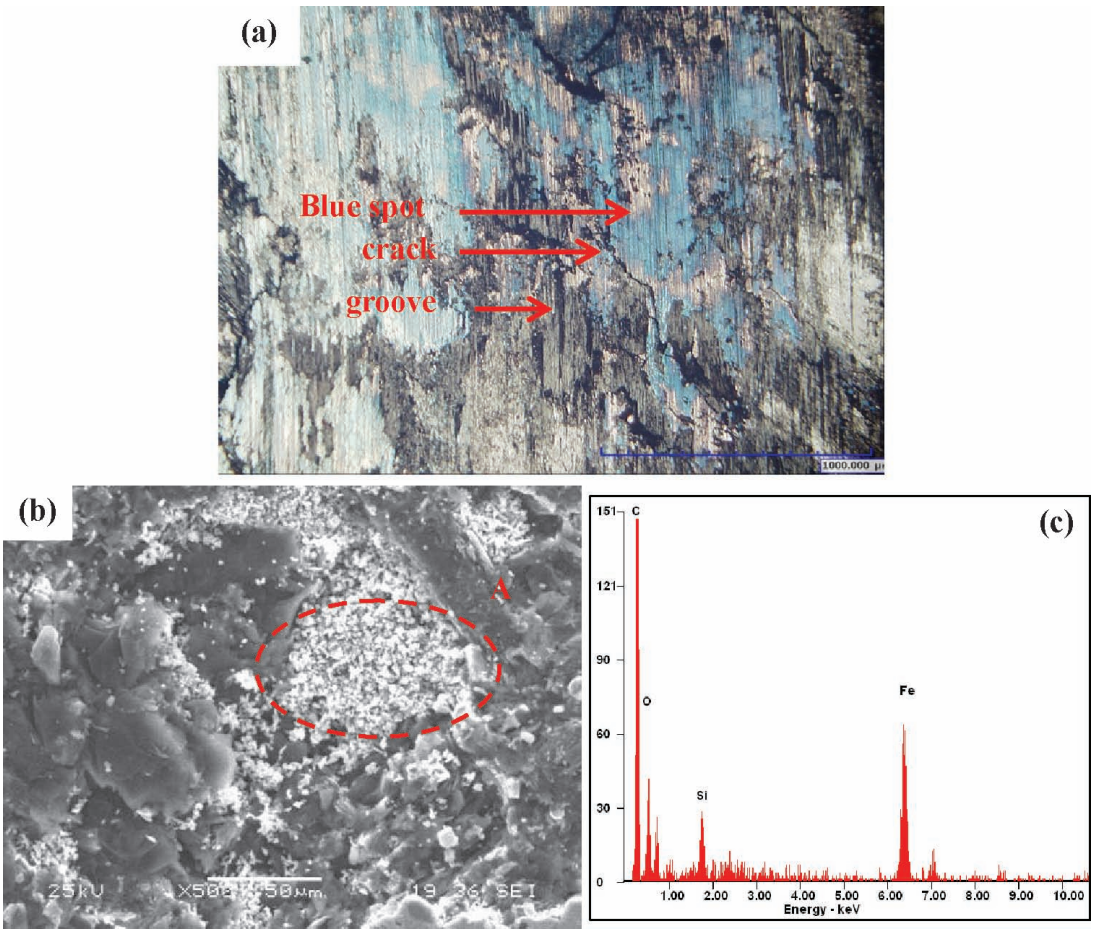


**Fig. 9:** Micrographs of typical worn surface of C/C-SiC modified with Fe-Si alloy: (a) worn surface morphology; (b) SEM micrograph; (c) EDS spectrum of point A in (b).

Blue spots indicate Fe was oxidized. The temperature of the subsurface of C/C-SiC modified with Fe-Si alloy was 344 °C. Thus, it could be reasonably inferred that the temperature of the friction surface is even higher. According to the study of Li *et al.* [14], the temperature of the friction surface could reach 600 °C at the later stage of each brake process, for some local "hot spots" on the friction surface, the temperature could even exceed 800 °C. Fan *et al.* [22] indicated that part of Fe in the debris was oxidized into $Fe_3O_4$ and FeO. In addition, according to the study of Li [15], Si could also be oxidized to $SiO_2$. Fig. 9(b) shows that broken asperities as wear debris fill the valley on the surface. As shown in Fig. 9(c), the EDS spectrum of the wear debris confirms that it contains Fe and O besides C and Si elements, which indicates the formation of $SiO_2$, FeO and $Fe_3O_4$.

Cracks, referred to as "fatigue cracks", are generated by cyclic stress and propagate merely in the friction films. During braking, asperities on the dual friction surface were sheared and pulverized to form a lot of granular debris. The debris filled the valleys to form a friction film for Van der Waals force, which is a weak binding force. In the course of braking, high local compressive stress and frictional traction forces were repeated a large number of times on the friction surface. Consequently, the friction film tore and cracks were generated. Moreover, the forming and breaking of friction film was in a dynamic state.

## IV. Conclusions

In order to obtain a stable COF of C/C-SiC composites at high brake speed, simultaneous infiltration of molten Si and Fe into needled C/C materials was developed for fabricating C/C-SiC composites. Microstructure, mechanical properties and tribological properties were characterized. Based on the investigation performed, the following conclusions could be drawn:

(1) The XRD result showed that C/C-SiC composites were composed of C, SiC, FeSi and $FeSi_2$, respectively. Furthermore, SiC and Fe-Si alloy was mainly located in short woven web cloth and among fiber bundles. SiC facilitated the infiltration of the Fe-Si into pores. Fe-Si alloy, far away from PyC, was only surrounded by SiC, owing to its good wetting ability with SiC.

(2) The compressive and flexural strength of C/C-SiC composites modified with Fe-Si alloy were 296.9 ± 15 MPa and 189.7 ± 20 MPa respectively, which were only 88.4 % and 85.7 % of the values for the unmodified C/C-SiC composites. The lower strength of the composites was attributed to the lower strength of the Fe-Si alloy and the weak Fe-Si alloy/SiC interfaces.

(3) The COF of the C/C-SiC composites modified with Fe-Si alloy mated with 30CrSiMoVA was 0.25 at speed of 25 m/s under 1 MPa pressure. The linear wear rate of C/C-SiC composites modified with Fe-Si alloy and steel counterpart were 3.4 μm/cycle and 3.2 μm/cycle, respectively. The lower hardness of the Fe-Si alloy compared to that of SiC was the main cause that led to improved friction characteristic, whereas the higher wear rate was attributable to the weak Fe-Si alloy/SiC interfaces. The typical brake curves were in the shape of a horse saddle.

## Acknowledgements

The authors are indebted to Yang Li and Rong Mei Fu for contributing their works. The authors gratefully acknowledge the financial support from the National Natural Science Foundation of China (Grant No. 51575536), Natural Science Foundation of Hunan Province (Grant No. 2015JJ3163), Science and Technology Program of Hunan Province (Grant No. 2015RS4016) and Nonferrous Metal Oriented Advanced Structural Materials and Manufacturing Cooperative Innovation Center in Central South University.

## References

1 Cai, Y., Yin, X., Fan, S., Zhang, L., Cheng, L.: Tribological behavior of three-dimensional needled ceramic modified carbon/carbon composites in seawater conditions, *Compos. Sci. Technol.*, **87**, 50 – 57, (2013).

2 Gadow, R., Kienzle, A.: Processing and manufacturing of C-fiber reinforced SiC- composites for disk brakes. In: Proceedings of the 6th International Symposium on Ceramic Materials and Components for Engines, Arita, Japan, 1997.

3 Krenkel, W., Henke, T.: Design of high performance CMC brake disks, *Key Eng. Mater.*, **164**, 421 – 424, (1999).

4 Krenkel, W.: CMC materials for high performance brakes. In: Proceedings of the ISATA Conference on Supercars. Aachen, Germany, 1994.

5 Krenkel, W., Heidenreich, B., Renz, R.: C/C-SiC composites for advanced friction systems, *Adv. Eng. Mater.*, **4**, 427 – 436, (2002).

6 Xiao, P., Li, Z., Xiong, X., Huang, B.: Preparation and tribological properties of C fibre reinforced C/SiC dual matrix composites fabrication by liquid silicon infiltration, *Solid State Sci.*, **16**, 6 – 12, (2013).

7 Xu, X., Fan, S., Zhang, L., Du, Y., Cheng, L.: Tribological behavior of three-dimensional needled carbon/silicon carbide and carbon/carbon brake pair, *Tribol. Int.*, **77**, 7 – 14, (2014).

8 Krenkel, W.: C/C-SiC composites for hot structures and advanced friction system, *Ceram. Eng. Sci. Proc.*, **24**, 583 – 592, (2003).

9 Xiao, P., Li, Z., Zhu, Z., Xiong, X.: Preparation, properties and application of C/C-SiC composites fabricated by warm Compacted-in situ reaction, *J. Mater. Sci. Technol.*, **26**, 283 – 288, (2010).

10 Fan, S., Zhang, L., Cheng, L., Tian, G., Yan, S.: Effect of braking pressure and braking speed on the tribological properties of C/SiC aircraft brake materials, *Compos. Sci. Technol.*, **70**, 959 – 965, (2010).

11 Cai, Y., Yin, X., Fan, S., Zhang, L., Cheng, L., Wang, Y., Yin, H.: Effects of particle sizes and contents of ceramic fillers on tribological behavior of 3D C/C composites, *Ceram. Int.*, **40**, 14029 – 14037, (2014).

12 Zhang, J., Fan, S., Zhang, L., Cheng, L., Yang, S., Tian, G.: Microstructure and frictional properties of 3D needled C/SiC brake materials modified with graphite, *Trans. Nonferrous Met. Soc. China*, **20**, 2289 – 2293, (2010).

13 Fan, X., Yin, X., He, S., Zhang, L., Cheng, L.: Friction and wear behaviors of C/C-SiC composites containing $Ti_3SiC_2$, *Wear*, **274 – 275**, 188 – 195, (2012).

14 Li, Z., Xiao, P., Zhang, B., Li, Y., Lu, Y.: Preparation and tribological properties of C/C-SiC brake composites modified by *in situ* grown carbon nanofibers, *Ceram. Int.*, **41**, 11733 – 11740, (2015).

15 Li, Z., Liu, Y., Zhang, B., Lu, Y., Li, Y., Xiao, P.: Microstructure and tribological characteristics of needled C/C-SiC brake composites fabricated by simultaneous infiltration of molten si and cu, *Tribol. Int.*, **93**, 220 – 228, (2016).

[16] Fan, S., Du, Y., He, L., Yang, C., Liu, H.: Microstructure and properties of α-$FeSi_2$ modified C/C-SiC brake composites, *Tribol. Int.*, **102**, 10 – 18, (2016).

[17] Ohnuma, I., Abe, S., Shimenouchi, S., Omori, T., Kainuma, R., Ishida, K: Experimental and thermodynamic studies of the fe-si binary system, *ISIJ International*, **52**, 540 – 548, (2012).

[18] Pan, Y., Gao, M.X., Oliveira, F.J., Vieira, J.M., Baptista, J.L.: Infiltration of SiC preforms with iron silicide melts: microstructures and properties, *Mater. Sci. Eng. A*, **359**, 343 – 349, (2003).

[19] Liu, G.W., Muolo, M.L., Valenza, F., Passerone, A.: Survey on wetting of SiC by molten metals, *Ceram. Int.*, **36**, 1177 – 1188, (2010).

[20] Fitzer, E., Gadow, R.: Fiber-reinforced silicon carbide, *Am. Ceram. Soc. Bull.*, **65**, 326 – 335, (1986).

[21] Li, H., Hausner, H.: Reactive wetting in the liquid-silicon/Solid-carbon system, *J. Am. Ceram. Soc.*, **79**, 873 – 880, (1996).

[22] Fan, S., Zhang, J., Zhang, L., Cheng, L., Tian, G., Liu, H.: Tribological properties of short fiber C/SiC brake materials and 30CrSiMoVA mate, *Tribology Lett.*, **43**, 287 – 293, (2011).